catalysts

MDPI

Article

Low-Temperature Synthesis of Anatase/Rutile/Brookite TiO_2 Nanoparticles on a Polymer Membrane for Photocatalysis

Kristina Fischer [1], Alina Gawel [1], David Rosen [2], Maria Krause [1], Amira Abdul Latif [1], Jan Griebel [1], Andrea Prager [1] and Agnes Schulze [1,*]

[1] Leibniz-Institute of Surface Modification, Permoserstr. 15, D-04318 Leipzig, Germany; kristina.fischer@iom-leipzig.de (K.F.); Alina.Gawel@web.de (A.G.); maria.krause@iom-leipzig.de (M.K.); amira.abdullatif@iom-leipzig.de (A.A.L.); jan.griebel@iom-leipzig.de (J.G.); andrea.prager@iom-leipzig.de (A.P.)

[2] Department of Civil and Environmental Engineering, Duke University, Durham, NC 27708, USA; david.rosen@duke.edu

* Correspondence: agnes.schulze@iom-leipzig.de; Tel.: +49-341-235-2400

Received: 31 May 2017; Accepted: 4 July 2017; Published: 10 July 2017

Abstract: Removing pollutants from water by using the photocatalyst TiO_2 is a highly-promising method. A large amount of work has been done to increase the activity of TiO_2, whereas the main two findings are increasing the surface area and applying mixed phase modifications (anatase, brookite, and rutile). Here, we present a method to directly synthesize non-agglomerated TiO_2 nanoparticles with different crystal phase ratios via low temperature dissolution-precipitation (LTDRP) on a porous microfiltration membrane (polyethersulfone). The amount of hydrochloric acid and the temperature was varied between 0.1–1 M and 25–130 °C, respectively, while the concentration of titanium precursor (titanium(IV) isopropoxide) was kept unchanged. The TiO_2 nanoparticles and the membrane were thoroughly characterized using X-ray diffraction (XRD), X-ray photoelectron spectroscopy (XPS), measuring the water contact angle and permeation flux, and examining the degradation of methylene blue. The mixed phase anatase/brookite with a main component being anatase exhibited the highest photocatalytic activity in removing methylene blue. Higher synthesis temperature induces enhanced crystallinity and, subsequently, the degradation rate of methylene blue was improved. Additionally, the photocatalytic activity remains high and unchanged for up to nine repeated cycles, i.e., full recovery of the photocatalytic properties is sustained.

Keywords: TiO_2 nanoparticles; photocatalysis; mixed phase; membrane reactor

1. Introduction

Water is one of the most important resources for humans and animals, but with a growing population it becomes more and more contaminated by chemicals, such as cleaning agents, personal care products, sweetening agents, insecticides, herbicides, and pharmaceuticals [1–3]. These organic micropollutants reach the water system from different origins, like human urine and feces, incorrect waste removal, waste water, or from industries [2]. Although the reported concentrations found in surface waters are at low concentrations (ng L^{-1} to mg L^{-1} range), undesired physiological effects for humans and animals cannot be neglected [2]. The current waste water treatment plants were not designed to purify water from many emerging contaminants (ECs), so that a constant entry is inevitably. There is a high demand for the development of intelligent systems to remove ECs from waste water. A fourth treatment stage, at the end of the waste water treatment, could remove ECs from water.

Advanced oxidation processes (AOPs, for example ozone, hydrogen peroxide, and titanium dioxide) efficiently clean waste water of organic micropollutants by mineralizing the organic molecules to water and carbon dioxide. The degradation is based on the generation of hydroxyl radicals, which oxidize organic molecules effectively and non-selectively [4]. The heterogeneous photocatalyst titanium dioxide (TiO_2) holds many advantages over other AOPs, like its photo and chemical stability, nontoxicity, reusability, and its low price [4].

TiO_2 can be either applied as a suspension [5] or bound to a support material e.g., on membranes [6], on carbon nanotube arrays [7], or on graphene oxide nanosheets [8]. The advantage of a supported TiO_2 system is that TiO_2 does not need to be extensively removed from the cleaned water. A suspension shows higher surface area compared to bound TiO_2, but taking a porous material like a polymer membrane as a support will increase the overall surface area [9]. The surface loss effect of a supported TiO_2 system is decreased. Additionally, the molecules to be degraded are transported directly to the surface of TiO_2 using a membrane reactor, and the removal of pollutants is enhanced.

Next to the surface area the crystallite type also significantly impacts the resulting photocatalytic activity [10]. Amorphous TiO_2 is not photoactive [11]. TiO_2 possesses three different types of modifications, namely anatase, rutile, and brookite [4]. Anatase is considered to have a higher photocatalytic activity compared to rutile, although the band gap is larger (3.2 eV for anatase vs. 3.0 eV for rutile) [12,13]. However, anatase, as an indirect band gap semiconductor (rutile is a direct band gap semiconductor), exhibits a longer lifetime for photo-excited electrons and holes. Additionally, anatase possesses a lower average effective mass of photo-generated electrons and holes. Therefore, these electrons and holes can migrate with a fast rate from the bulk to the surface, which results in a low recombination rate [13]. Few studies observed the photocatalytic activity of brookite as the synthesis of pure brookite is technically difficult [14]. In these studies [15–17] brookite is described as a better photocatalyst compared to anatase and rutile because electrons are trapped at moderate depths, so that both electrons and holes are still accessible for reduction and oxidation reactions. Generally, a mixture of these modifications gives higher photocatalytic activities due to synergistic effects like interfacial electron transfer [12,18–22]. With a mixture of anatase and rutile the recombination of photo-generated electrons and holes is reduced, and the absorption of light is increased by rutile [12,18,19]. A mass ratio of 3:7 (rutile to anatase) gives best photocatalytic activities [18]. A mixture of anatase and brookite, as well as rutile and brookite, has also been observed to gain fast degradation rates of organic molecules via photocatalysis [20,21].

Most methods deposit TiO_2 nanoparticles in a separate process on the membrane [23–28] or embed it directly in the membrane casting solution [29–36]. Disadvantages of the mentioned methods are aggregation of nanoparticles [9,26,28,37] and high sealing of nanoparticles in the bulk of the membrane polymer [9,23], respectively. The direct synthesis of TiO_2 nanoparticles on a membrane via hydrolysis of titanium alkoxides leads to finely- and evenly-distributed nanoparticles [9,37]. However, a separate step has to be included as the synthesized TiO_2 is amorphous and, therefore, not photocatalytically active. Crystallization is often performed by calcination at temperatures above 400 °C [12,18,19,38], but would degrade the supporting membrane material. Low-temperature crystallization with water [18,39–41] is a low-cost alternative compared to calcination. Water acts as a catalyst linking TiO_6^{2-} octahedra together to share edges leading to anatase [18,39–41]. Additionally, calcination of anatase to rutile at high temperatures (>500 °C) leads to agglomeration of nanoparticles, i.e., lower surface area [42–44]. However, only the crystal form of anatase was generated and, as stated above, a mixed phase is aspired to increase photocatalytic performance.

Here, we enhanced the synthesis to gain a mixture of TiO_2 phases (namely anatase, rutile, and brookite) of nanoparticles on a polyethersulfone (PES) membrane. The photocatalytic activity, i.e., the reaction rate constant, increased by more than three times compared to the membrane with pure anatase TiO_2 nanoparticles [9]. Additionally, the TiO_2 nanoparticle membrane completely degraded methylene blue for nine repeated cycles. TiO_2 nanoparticles were synthesized via hydrolysis (low temperature dissolution-precipitation LTDRP) [42,45] of titanium alkoxide using hydrochloric acid

(HCl) in different concentrations and at various temperatures ranging from 0.1 M to 1 M and 25 °C to 130 °C, respectively.

The membranes modified with TiO_2 were thoroughly characterized. The morphology was examined via scanning electron microscopy (SEM), the TiO_2 content with X-ray photoelectron spectroscopy (XPS), the hydrophilic properties by water contact angle measurement, the crystal composition via X-ray diffraction (XRD), the water permeation with dead-end filtration setup, and the photocatalytic activity by degrading methylene blue (MB).

2. Results and Discussion

2.1. Crystal Phase

The formed crystal composition depends on the acid concentration and temperature used during synthesis. Changing the amount of titanium alkoxide [46] and time of reaction [47] also has an impact on the crystal composition, but was not investigated here. The three TiO_2 modifications develop due to a different linking of the TiO_6^{2-} octahedra [22,42,46–48] either by a solid-state rearrangement (anatase) or by a dissolution precipitation reaction (rutile) [49]. Anatase consists of edge-sharing TiO_6^{2-} octahedra, rutile shares an edge along the *c* axis to form chains and corner-shared bonding among these chains, and brookite is more complicated as it shares edges and corners [46]. The mechanism of crystal forming by combining TiO_6^{2-} octahedra has been discussed elsewhere and includes different theories using a thermodynamic and kinetic approach [47,50] or looking at the amount of OH^- present at different conditions [42,48].

The crystalline phase type was observed with XRD. Direct measurement of TiO_2 nanoparticles on the membrane is not possible as the amount of TiO_2 in comparison to the support PES membrane is too low and the membrane surface too rough to use a small incident angle. Therefore, the remaining non-attached TiO_2 nanoparticles were analyzed. The generated TiO_2 nanoparticles contained the phase type anatase, brookite, and rutile according to the adjusted acid concentration and temperature (Figure 1). Acid concentration as well as the temperature has a major impact on the formed crystal composition because the kinetics of reactions taking place was changed and the amount of OH^- was varied by temperature and acid [42,46,50].

At 90 °C (Figure 1a,c) the anatase and brookite content decreased from 60% to 4% and 24% to 0%, respectively, and the rutile portion increased from 15% to 96% by raising the acid concentration from 0.25 to 1 M. A similar behavior was observed at 120 °C and 130 °C. Thus, it appears that at higher acid concentrations the formation of rutile is favored. Brookite was formed at intermediate concentrations of acid and vanished before anatase to form rutile. A similar behavior was found in the literature [47]. At lower acidity more OH^- ligands are formed, so that edge-sharing of TiO_6^{2-} octahedra is much more likely to occur during dehydration reactions and anatase is formed [46]. With higher acidity the amount of OH^- ligands is lower. Edge-shared bonding is minimized because it needs two dehydration reactions taking place at the same time. Corner-sharing takes place more easily to gain rutile phase [46]. Another approach explaining the different effects of acid considers the different mechanism of crystallization, i.e., comparing the solid-state mechanism leading to anatase and the dissolution precipitation mechanism leading to rutile [49]. With increasing acid concentration, the surface of titania becomes protonated and titania solubilized. A dissolution precipitation process is possible so that rutile is formed [49].

At low temperatures (room temperature and 60 °C) the impact of acid concentration was less pronounced. At high acid concentration (0.5 and 1 M) only rutile was formed. With 0.25 M HCl the sample was either amorphous (room temperature: RT) or yielded 84% of anatase and 26% of rutile (no brookite). The amount of OH^- ions in water is changing with temperature, according to the equilibrium law (Le Chatelier's principle). The dissociation of water is an endothermic process. At room temperature the concentration of OH^- is at $[OH^-] = 2 \times 10^{-14}$ M with an acid concentration of $[H^+] = 0.5$ M. Increasing the temperature to 130 °C will increase the concentration of OH^- by about

119 times ([OH^-] = 2.4 × 10^{-12} M). The increase is not linear (ionic product K_w at 25 °C is 1 × 10^{-14} M^2, at 60 °C about 10 × 10^{-14} M^2 at 90 °C about 30 × 10^{-14} M^2, at 120 °C about 93 × 10^{-14} M^2, and at 130 °C about 119 × 10^{-14} M^2) [51]. Thus, at lower temperatures (here, at room temperature and at 60 °C) the amount of OH^- is low and, therefore, edge-sharing is preferred to form rutile. With an acid concentration of 0.25 M the OH^- concentration is still high enough to form anatase next to rutile. At room temperature the crystallization was too slow to form crystallites [50]. Longer reaction time would generate also crystals of TiO_2. With higher acid concentration or temperature the crystallization rate is increased and crystal structures occurred.

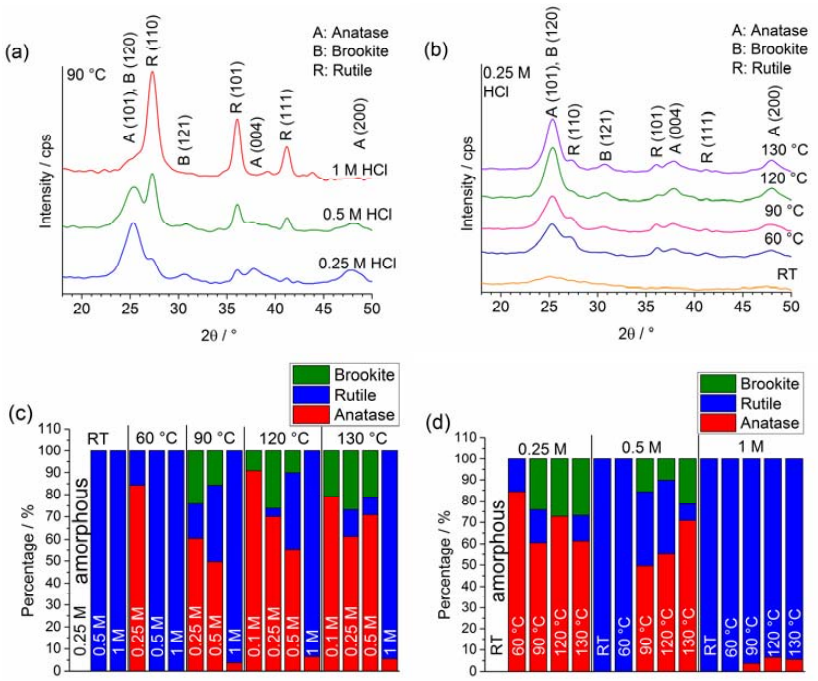

Figure 1. XRD (X-ray diffraction) pattern ((**a**,**b**) smoothened with a 17 point FFT (fast Fourier transform) filter) and the percentage of phase type (**c**,**d**) of TiO_2 powder prepared at different temperatures and with different acid concentrations. In (**a**) the acid concentration was increased and the temperature stayed constant at 90 °C. In (**b**) the temperature was changed and the acid concentration was kept at 0.25 M.

Changing the temperature affects also the crystal composition (see Figure 1b,d). Again, a critical change occurred between 60 and 90 °C. At low acid concentration (0.25 M) the composition changed from amorphous (RT), to anatase-rutile (60 °C, 84% and 16%, respectively). At higher temperatures (90, 120, and 130 °C) also brookite was formed and the composition did not change in between 90, 120 °C, and 130 °C, significantly (anatase-brookite-rutile 90 °C: 61-24-15%; 120 °C: 70-26-4%; 130 °C: 61-27-12%). At a concentration of 0.5 M HCl only rutile was formed at room temperature and 60 °C, while at higher temperatures (90, 120, and 130 °C), next to rutile, anatase and brookite were also generated. With a high acid concentration (1 M) again only rutile was developed at temperatures below 60 °C. At temperatures above 90 °C a small amount of anatase was also generated, in addition to rutile.

Overall, only rutile occurs alone (high acid concentration and low temperature). Brookite appears ternary in combination with both anatase and rutile or just in combination with anatase (high temperatures and low acid concentration). Brookite is more easily transformed to rutile than anatase [47]. Therefore, brookite disappears first before anatase is transformed to rutile. Anatase was found to be formed together with rutile (high acid concentration and high temperature, as well as at 60 °C and 0.25 M HCl).

The crystal size of anatase, brookite, and rutile was calculated by the Scherrer formula. Overall the crystal size was growing with increased temperature and acid concentration (Supplementary Materials,

Figure S1). As the anatase crystals grow larger, they become unstable. Anatase crystals migrate and align so that an in situ rearrangement of the lattice transforms them to rutile crystallites [52]. High acid concentrations, as well as large temperatures, accelerate crystal growth.

2.2. Morphology and the Amount of TiO_2

TiO_2 nanoparticles of different shape and quantity have been directly synthesized on a PES membrane. The temperature and acid concentration during synthesis had an impact on the above mentioned values.

The amount of TiO_2 on the membrane clearly increased with elevated temperatures (Figures 2 and 3). The reprecipitation of TiO_2 was increased with higher temperatures and led to a higher content of TiO_2 on the membrane surface [43]. A trend of TiO_2 content with changing acid concentration is not clearly pronounced (Figure 3). At high temperatures (120 and 130 °C) the amount of TiO_2 was increased, while the acid concentration was raised from 0.1 M to 0.25 M HCl. Further increasing of the acid concentration led to a decrease of TiO_2 at high temperatures (120 and 130 °C). At temperatures of 60 and 90 °C the amount of TiO_2 was elevated with increasing acid concentration. The used concentration of HCl during synthesis changed the shape of the generated TiO_2 nanoparticles (Figure 2). At a HCl concentration of 0.25 M primarily spherical particles were formed. Only at 60 °C were rod-like particles also detected. Increasing the HCl concentration to 0.5 M produced spherical and rod-like particles, which can also be observed at HCl concentrations of 1 M at all temperatures. The rod-like particles formed flower-like structures (see Figure 2, e.g., 130 °C, 1 M HCl). The formation of rod-like particles is typically described in the literature for rutile [17,46,53], the generation of flower-like structures is known [46]. XRD (see Section 2.1) proves the assumption of the formation of rutile at higher concentrations of HCl.

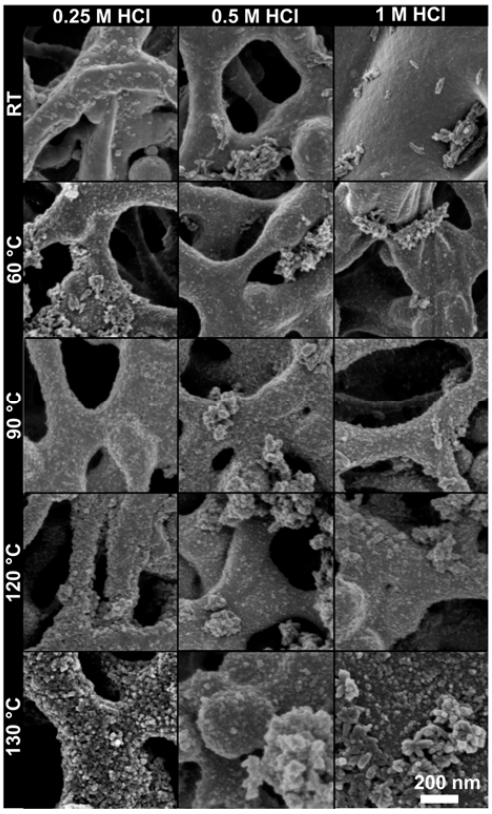

Figure 2. SEM (scanning electron microscopy) image of PES (polyethersulfone) membranes with TiO_2 nanoparticles synthesized at different temperatures (room temperature: RT, 60 °C, 90 °C, 120 °C, and 130 °C) and with different concentrations of HCl (0.25 M, 0.5 M, and 1 M).

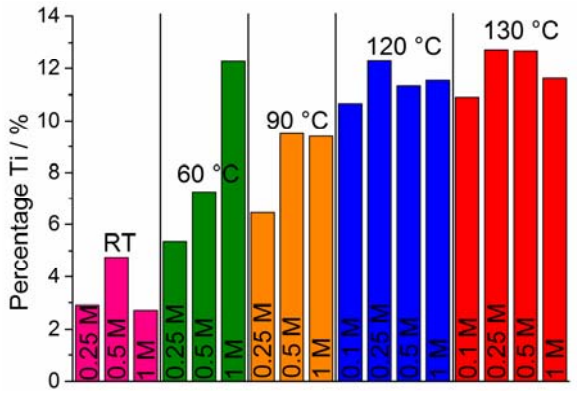

Figure 3. Titanium content in percentage on the PES membranes with TiO_2 nanoparticles synthesized at different temperatures (RT, 60 °C, 90 °C, and 130 °C) and with different amounts of HCl (0.25 M, 0.5 M, and 1 M) measured with XPS.

2.3. Hydrophilicity and Water Permeation Flux

The hydrophilicity of the membranes with TiO_2 nanoparticles was evaluated by measuring the water contact angle on the membrane surface (Figure 4a). TiO_2 is a well-known additive to increase the hydrophilicity [36]. The amount of hydroxyl groups on the surface affects the water contact angle [54]. The unmodified membrane can be classified as hydrophilic with a value below 90° [55]. With increasing treatment temperature the water contact angle decreased, i.e., the hydrophilicity was enhanced. Values below 20° were observed for samples treated at temperatures above 90 °C. The structural morphology change visualized by SEM imaging (Figure 2) could be a reason for the change in contact angle. Structural changes have a high impact on the contact angle, which is widely described in the literature [54,56,57].

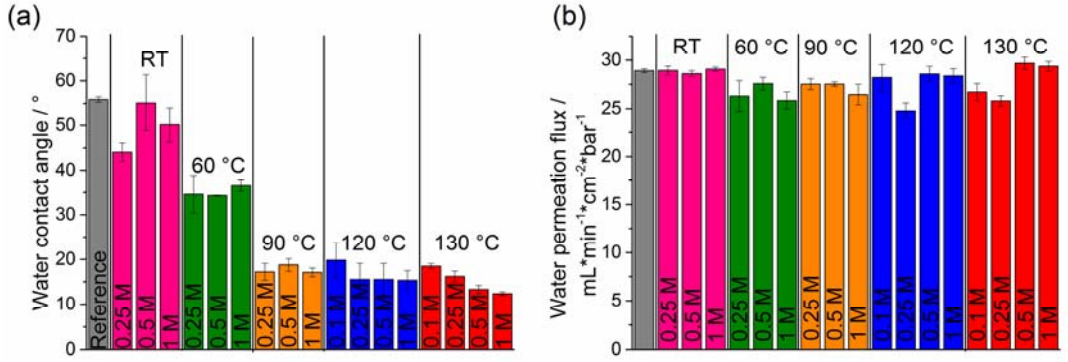

Figure 4. Water contact angle (**a**) and water permeation flux (**b**) of the unmodified membrane (Reference) and membranes with TiO_2 nanoparticles generated at different temperatures and acid concentrations.

The generation of TiO_2 nanoparticles on the membrane did only reduce the water permeation flux by a small value (Figure 4b). An addition of TiO_2 nanoparticles on the membrane surface (also inner surface) should reduce the pore diameter, which would decrease the permeation flux. This effect was not observed here and can be explained by an increase in hydrophilicity (Figure 4a). Two competitive factors (hydrophilicity and pore narrowing) influence the flux, so that in sum the permeation flux did not change significantly.

2.4. Photocatalytic Activity

The photocatalytic activity was determined by degrading methylene blue over time. Methylene blue is widely used as a model compound for photocatalytic tests.

First the adsorption of methylene blue was studied, as the adsorption already influences the photocatalytic activity (i.e., high adsorption → high surface area and high photocatalytic activity) [58]. Methylene blue is a cationic dye, which will preferably adsorb on negatively charged surfaces. TiO_2 is negatively charged in the methylene blue solution (pH 8.5) with an isoelectric point (IEP) below 6.2 [59]. Starting at a synthesis temperature of 60 °C, the adsorption of methylene blue increased with the used temperature and acid concentration during synthesis of the TiO_2 nanoparticles (Figure 5a). The TiO_2 nanoparticles synthesized with the method from Fischer et al. [9] adsorb 21% of methylene blue, which can be increased to 39% with the synthesis method described here (1 M HCl and 130 °C). The variation in methylene blue adsorption can originate from a difference in surface area, IEP, and value of zeta potential. The raising content of TiO_2 (Figure 3) and the morphology change with increasing temperature and acid concentration (Figure 2) enhances the surface area, hence, more methylene blue was adsorbed. Additionally, the IEP and zeta potential (negative) decrease with the increasing particle size [59]. Due to the increasing acid concentration larger particles (rod-like particles, Figure 2 and supplementary Materials, Figure S1) were formed, and the zeta potential and IEP [59] decreased. Therefore, the adsorption of the cationic methylene blue dye increased. Additionally, the shape of the crystals has an influence on the adsorption, as the planar facets of the rutile crystals allows the alignment of an increased amount of adsorbed molecules on the surface [17].

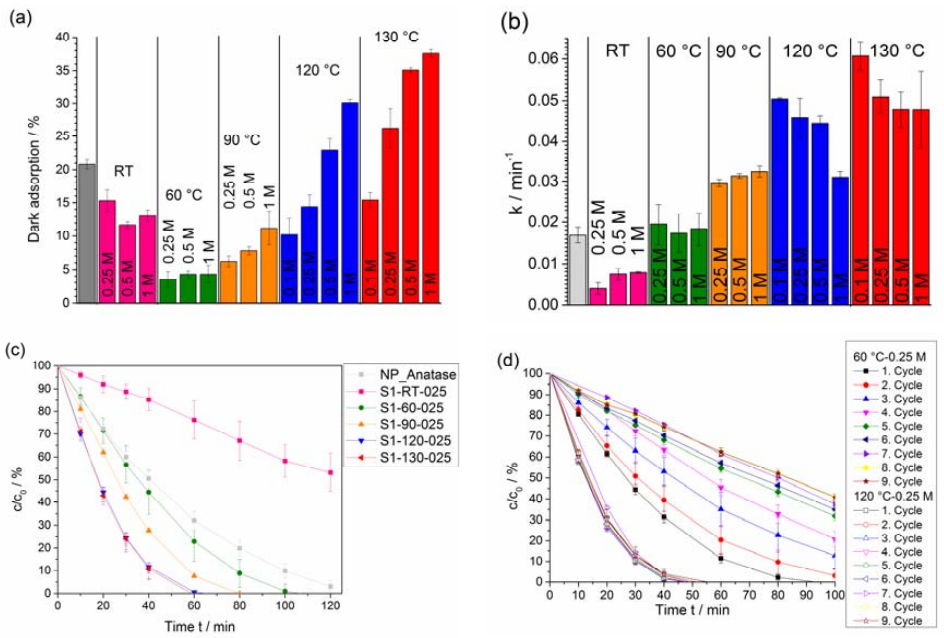

Figure 5. Methylene blue adsorption (**a**), reaction rate constants of the photocatalytic degradation of methylene blue (**b**), and photocatalytic degradation of methylene blue over time (**c**) for the membrane with TiO_2 nanoparticles generated at different temperatures and acid concentrations and the membrane with TiO_2 nanoparticles formed according to the method from Fischer et al. (NP_Anatase) [9]. In (**d**) the photocatalytic degradation of methylene blue over time is shown for up to nine cycles of the membrane with TiO_2 nanoparticles synthesized at 60 and 120 °C and with 0.25 M HCl.

The degradation of methylene blue was dependent on the temperature and acid concentration at which the TiO_2 nanoparticles have been synthesized on the membrane (Figure 5b,c). The reaction rate constant of the degradation of methylene blue was calculated by plotting $\log(c/c_0)$ versus time and estimating the slope of the regression line. A high rate constant implies fast degradation of methylene

blue. With increasing temperature the rate constant was enhanced. The rate constant was raised from a minimal value of 0.004 min^{-1} (room temperature and 0.25 M HCl) to 0.0607 min^{-1} (130 °C and 0.1 M HCl). After 60 min methylene blue was completely degraded with a TiO_2 nanoparticle membrane synthesized at 120 and 130 °C while the membrane with TiO_2 nanoparticle produced at room temperature removed only 24%. With higher synthesis temperatures the reflections of the XRD pattern was narrower (Figure 1b) indicating higher crystallinity. Increasing the crystallinity will reduce the formation of electron traps, so that fewer recombination centers of photogenerated electrons and holes are created [60]. Hence, the photocatalytic activity will be improved. Increasing the temperature further on could increase the crystallinity and photocatalytic activity. However, the chosen support (PES membrane) would be damaged if temperatures above 130 °C are applied.

The acid concentration influences the photocatalytic activity at higher temperatures (120 and 130 °C). The rate constant was decreased with raising acid concentration. At 120 °C the rate constant decreased from 0.0504 min^{-1} (0.1 M HCl) to 0.0309 min^{-1} (1 M HCl). The trend of degradation was contrary to the adsorption of methylene blue (Figure 5a,b). Higher adsorption would usually lead to higher photocatalytic activity as the affinity of methylene blue to TiO_2 and/or the surface area of TiO_2 is enhanced. However, the crystal phase composition also has an impact on the photocatalytic activity. A combination of a high content in anatase (91%) and low content of brookite (9%) enhances the photocatalytic activity (130 °C and 0.1 M HCl). A combination of brookite and anatase have been reported in the literature to have higher photocatalytic activity compared to pure anatase [20] and triphasic composites additionally containing rutile [22]. Pure brookite and anatase have been described to have a similar degradation rate and a much higher photocatalytic activity than rutile [17]. A combination of these two crystals (anatase and brookite) has a synergistic effect as the electron transfer between these two faces is enhanced [22].

The reduction of methylene blue was repeated for up to nine cycles (see Figure 5d) with two differently modified membranes (60 and 120 °C, 0.25 M HCl). The TiO_2 nanoparticles on the membrane synthesized at 120 °C do not show any activity loss over nine cycles. This is in contrast to the TiO_2 nanoparticles produced at 60 °C on the membrane as the reduction of methylene blue gradually deteriorates with repeating degradation runs. This membrane does not regain its white color after the first cycle and the membrane is colored deep blue after nine cycles (see Figure 6). Methylene blue is still adsorbed at the membrane surface while the membrane with TiO_2 nanoparticles synthesized at 120 °C is white after the first cycle and light blue after the ninth cycle (Figure 6). Although the membrane with TiO_2 nanoparticles produced at 120 °C turns light blue after nine cycles the photocatalytic activity is not declined and full recovery of the photocatalytic properties is given. An indirect proof for the stability of the membrane against an attack from $OH^{\bullet}$ radicals was obtained for the membrane synthesized with TiO_2 nanoparticles at 120 °C as the photocatalytic degradation rate was not changed after an irradiation for 900 min. An attack of $OH^{\bullet}$ radicals would have resulted in a change in photocatalytic activity. The TiO_2 nanoparticle film (synthesized at 120 °C) on the membrane acts as a protective layer as it totally covers the surface of the membrane [27]. It is well known that semiconducting photocatalysts can degrade carbon materials [61,62]. Therefore, a possible damage of the membrane material will be the focus of further studies.

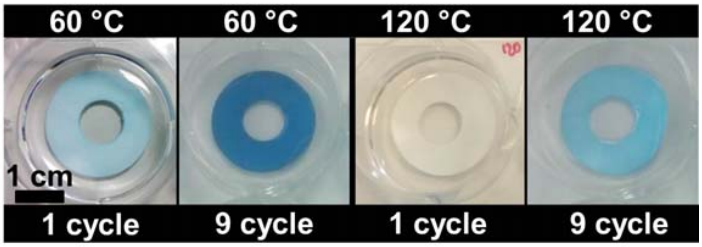

Figure 6. Photographic images of the membranes with TiO_2 nanoparticles (0.25 M HCl, 120 °C or 60 °C) after one cycle and nine cycles.

3. Materials and Methods

3.1. Materials

The PES membrane (0.22 µm, Millipore Express® PLUS membrane GPWP) was purchased from Merck Millipore, Billerica, MA, USA. Hydrochloric acid (37%) and titanium(IV) isopropoxide (TTIP, 97%) were acquired from Sigma-Aldrich, Steinheim, Germany and methylene blue (96+%) from Acros Organics (Fisher Scientific, Waltham, MA, USA). Milli-Q water was obtained from Milli-Q integral system (EMD Millipore, Billerica, MA, USA).

3.2. Nanoparticle Synthesis on the Membrane

The membranes were cut into pieces of 3 × 9 cm and two of them were put into a Teflon beaker. Thereby, the top side of the membrane (the side with smaller pores) was turned inward-looking. The beaker was filled with Milli-Q water (80 mL in total), TTIP (8.1 mL), and 37% hydrochloric acid. The amount of HCl depends on the used total concentration in the beaker varying from 0.1 to 1 M.

The beaker was closed and shaken for 4 h at room temperature. Afterwards, the membranes were tempered for 20 h at different temperatures in the beaker. After cooling, the membranes were washed with Milli-Q water by shaking 3 × 30 min. Subsequently, the membranes were dried in air.

The excessive TiO_2 suspensions were, depending on the particle size, either centrifuged or allowed to stand overnight to achieve sedimentation of the particles. The supernatant clear liquid was decanted and the sludge was blended with Milli-Q water and shaken for washing. After re-sedimentation and decantation, the sludge was dried, pestle, and used for XRD measurements.

3.3. Characterization

For SEM imaging, the samples were sputtered with a 30 nm chromium layer with a Leybold Z400 sputter system (Cologne, Germany). SEM images were taken with a Carl Zeiss Ltd. Ultra 55 SEM (Oberkochen, Germany). XPS spectra were measured at the Kratos Analytical Ltd. Axis Ultra (Manchester, UK) with a monochromatic Al Kα cathode. The X-ray source power was 150 W and the pass energy was 40 eV. To gain information about the crystal composition of the TiO_2 nanoparticles XRD measurements have been performed. It is not possible to directly perform XRD measurements of the TiO_2 layers on the membranes as the signals are superimposed by noise caused by the polymer structure of the membrane. Therefore, the excessive TiO_2 powder in suspension was refined after synthesis and used for XRD. The XRD patterns have been measured with a Rigaku Ultima IV X-ray diffraction spectrometer (Tokyo, Japan) with Cu Kα radiation (40 kV, 40 mA, scanning speed: 2 ° min^{-1}, step size: 0.05°). From the peak integrals A, the weight fractions W of the phases were calculated with Equations (1)–(3) using the response factors k (k_A = 0.886, k_R = 1 and k_B = 2.721) [22]:

$$W_A = \frac{k_A \cdot A_A}{k_A \cdot A_A + k_R \cdot A_R + k_B \cdot A_B} \quad (1)$$

$$W_R = \frac{k_R \cdot A_R}{k_A \cdot A_A + k_R \cdot A_R + k_B \cdot A_B} \quad (2)$$

$$W_B = \frac{k_B \cdot A_B}{k_A \cdot A_A + k_R \cdot A_R + k_B \cdot A_B} \quad (3)$$

The crystallite sizes of TiO_2 were determined by using Scherrer's equation:

$$d = 0.9\lambda / B \cos\theta \quad (4)$$

where d, λ, B, and θ are the crystallite size, Cu Kα wavelength (0.15418 nm), full width at half–maximum intensity (fwhm) of the reflection (anatase (101), brookite (121), and rutile (110)) in radians, and Bragg's diffraction angle, respectively [63]. For contact angle measurement a piece of modified membrane

was glued to an object slide. With a Krüss DSA 30E (Hamburg, Germany), a 2 µL water drop was placed on the surface. The process of drop deposition and permeation was tracked by a camera and the contact angle was determined from the video after the drop was completely placed on the membrane. This procedure was repeated on five areas of the membrane. For water permeation flux measurements, membrane circles with a diameter of d = 2.5 cm were cut and placed in a Sartorius 16249 pressure filter holder (Göttingen, Germany). The time for 100 mL of Milli-Q water passing through the membrane at an applied nitrogen pressure of p = 1 bar was measured. For each sample three membrane pieces were tested. From the measured time, the water permeation flux J could be calculated using Equation (5):

$$J = \frac{V}{t \times A \times p} \tag{5}$$

where J is the permeability (mL min^{-1} cm^{-2} bar), V is the volume (mL), t is time (min), A is the surface area of the membrane (cm^2), and p is the pressure (bar).

The procedure of the photocatalytic degradation test has been described elsewhere [9,64]. Briefly, a circle with the diameter d = 2.5 cm was cut from the membrane. An additional hole was cut in the middle of these circle (d = 1 cm). Three of these circles were glued into vicinal pits of six-well-plates. All six pits were filled with 4 mL of a 20 µM methylene blue solution in water. The zero value of the absorption by methylene blue was measured immediately with a Tecan Infinite M200 multimode microplate reader (Männedorf, Switzerland) at a wavelength of λ = 660 nm. The samples were shaken on a radial shaker with 200 rpm without irradiation to measure the dark adsorption for 30 min. The absorption of the solution was measured in 10 min intervals. Subsequently, the samples were irradiated with a sunlamp (Heraus Original Hanau Suncare tanning tube 21/25 slim, Hanau, Germany) to perform photocatalysis for 2 h. The radiant flux density of the lamp was 11.3 ± 1.3 mW cm^{-2}. For the first 40 min, the absorbance of the remaining methylene blue was measured every 10 min and, afterwards, every 20 min. The non-catalytic photolysis of methylene blue has been subtracted from the photocatalytic measurement. By plotting $log(c/c_0)$ versus the time, the observed reaction rate constants k could be derived from the slope of the regression line.

4. Conclusions

Non-agglomerated TiO_2 nanoparticles have been directly synthesized via low-temperature dissolution-precipitation on a microfiltration PES membrane with different crystallinities and varying crystal composition, including anatase, brookite, and rutile. For that purpose the amount of hydrochloric acid and reaction temperature was varied between 0.1–1 M and 25–130 °C, respectively, while the concentration of titanium precursor (titanium(IV) isopropoxide) was kept unchanged. The crystallinity and modification composition has an influence on the resulting photocatalytic activity. High crystallinity and a mixed phase of mainly anatase (79%) and a small amount of brookite (21%) give the best degradation rate of methylene blue. The photocatalytic activity was not declined and full recovery of the photocatalytic properties of at least nine repeated cycles was retained with a mixed phase sample containing anatase, brookite, and rutile (70%, 26%, and 4%, respectively) and having a high crystallinity. The degradation rate of pure rutile TiO_2 nanoparticles on a membrane with lower crystallinity subsequently declined over nine cycles. The permeation flux of the membrane did not change significantly, so that the membrane can be used for membrane reactors without any loss in flux. Additionally, the water contact angle of the membrane was improved to a value below 20° at synthesis temperatures above 60 °C. Thus, the membrane is highly suitable for water applications and low fouling can be expected. The implantation of this catalytic membrane in a reactor system for degradation of organic pollutants is highly promising.

Supplementary Materials: The following are available online at www.mdpi.com/2073-4344/7/7/209/s1. Figure S1. Crystal size of TiO_2 depending on temperature and acid concentration calculated by the Scherrer formula.

Acknowledgments: The financial support by the Federal State of Germany, the German Academic Exchange Service, and the Free State of Saxony is gratefully acknowledged.

Author Contributions: Kristina Fischer and Agnes Schulze conceived and designed the experiments; Kristina Fischer, Alina Gawel, David Rosen, Maria Krause, and Amira Abdul Latif performed the experiments; Jan Griebel performed the XRD, Andrea Prager performed the XPS and SEM, and Kristina Fischer and Alina Gawel analyzed the data; and Kristina Fischer wrote the paper.

Conflicts of Interest: The authors declare no conflict of interest. The founding sponsors had no role in the design of the study; in the collection, analyses, or interpretation of data; in the writing of the manuscript, and in the decision to publish the results.

References

1. Tijani, J.O.; Fatoba, O.O.; Babajide, O.O.; Petrik, L.F. Pharmaceuticals, endocrine disruptors, personal care products, nanomaterials and perfluorinated pollutants: A review. *Environ. Chem. Lett.* **2016**, *14*, 27–49. [CrossRef]
2. Archer, E.; Petrie, B.; Kasprzyk-Hordern, B.; Wolfaardt, G.M. The fate of pharmaceuticals and personal care products (PPCPs), endocrine disrupting contaminants (EDCs), metabolites and illicit drugs in a WWTW and environmental waters. *Chemosphere* **2017**, *174*, 437–446. [CrossRef] [PubMed]
3. Richardson, S.D.; Kimura, S.Y. Water analysis: Emerging contaminants and current issues. *Anal. Chem.* **2016**, *88*, 546–582. [CrossRef] [PubMed]
4. Kumar, J.; Bansal, A. Photocatalysis by nanoparticles of titanium dioxide for drinking water purification: A conceptual and state-of-art review. *Mater. Sci. Forum* **2013**, *764*, 130–150. [CrossRef]
5. Molinari, R.; Pirillo, F.; Loddo, V.; Palmisano, L. Heterogeneous photocatalytic degradation of pharmaceuticals in water by using polycrystalline TiO_2 and a nanofiltration membrane reactor. *Catal. Today* **2006**, *118*, 205–213. [CrossRef]
6. Sarasidis, V.C.; Plakas, K.V.; Patsios, S.I.; Karabelas, A.J. Investigation of diclofenac degradation in a continuous photo-catalytic membrane reactor. Influence of operating parameters. *Chem. Eng. J.* **2014**, *239*, 299–311. [CrossRef]
7. Saleh, T.A.; Gupta, V.K. Dedication. In *Nanomaterial and Polymer Membranes*; Elsevier: Amsterdam, The Netherlands, 2016.
8. Akhavan, O.; Ghaderi, E. Photocatalytic reduction of graphene oxide nanosheets on TiO_2 thin film for photoinactivation of bacteria in solar light irradiation. *J. Phys. Chem. C* **2009**, *113*, 20214–20220. [CrossRef]
9. Fischer, K.; Grimm, M.; Meyers, J.; Dietrich, C.; Gläser, R.; Schulze, A. Photoactive microfiltration membranes via directed synthesis of TiO_2 nanoparticles on the polymer surface for removal of drugs from water. *J. Membr. Sci.* **2015**, *478*, 49–57. [CrossRef]
10. Wang, Q.; Lian, J.; Bai, Y.; Hui, J.; Zhong, J.; Li, J.; An, N.; Yu, J.; Wang, F. Photocatalytic activity of hydrogen production from water over TiO_2 with different crystal structures. *Mater. Sci. Semicond. Process.* **2015**, *40*, 418–423. [CrossRef]
11. Henderson, M. A surface science perspective on TiO_2 photocatalysis. *Surf. Sci. Rep.* **2011**, *66*, 185–297. [CrossRef]
12. Liao, Y.; Que, W. Preparation and photocatalytic activity of TiO_2 nanotube powders derived by a rapid anodization process. *J. Alloys Compd.* **2010**, *505*, 243–248. [CrossRef]
13. Zhang, J.; Zhou, P.; Liu, J.; Yu, J. New understanding of the difference of photocatalytic activity among anatase, rutile and brookite TiO_2. *Phys. Chem. Chem. Phys.* **2014**, *16*, 20382–20386. [CrossRef] [PubMed]
14. Di Paola, A.; Bellardita, M.; Palmisano, L. Brookite, the least known TiO_2 photocatalyst. *Catalysts* **2013**, *3*, 36–73. [CrossRef]
15. Li, Z.; Cong, S.; Xu, Y. Brookite vs anatase TiO_2 in the photocatalytic activity for organic degradation in water. *ACS Catal.* **2014**, *4*, 3273–3280. [CrossRef]
16. Vequizo, J.J.M.; Matsunaga, H.; Ishiku, T.; Kamimura, S.; Ohno, T.; Yamakata, A. Trapping-induced enhancement of photocatalytic activity on brookite TiO_2 powders: Comparison with anatase and rutile TiO_2 powders. *ACS Catal.* **2017**, *7*, 2644–2651. [CrossRef]

17. Tran, H.T.T.; Kosslick, H.; Ibad, M.F.; Fischer, C.; Bentrup, U.; Vuong, T.H.; Nguyen, L.Q.; Schulz, A. Photocatalytic performance of highly active brookite in the degradation of hazardous organic compounds compared to anatase and rutile. *Appl. Catal. B Environ.* **2017**, *200*, 647–658. [CrossRef]
18. Yu, J.; Wang, B. Effect of calcination temperature on morphology and photoelectrochemical properties of anodized titanium dioxide nanotube arrays. *Appl. Catal. B Environ.* **2010**, *94*, 295–302. [CrossRef]
19. Kim, S.-J.; Lee, E.G.; Park, S.D.; Jeon, C.J.; Cho, Y.H.; Rhee, C.K.; Kim, W.W. Photocatalytic effects of rutile phase TiO_2 ultrafine powder with high specific surface area obtained by a homogeneous precipitation process at low temperatures. *J. Sol-Gel Sci. Technol.* **2001**, *22*, 63–74. [CrossRef]
20. Ozawa, T.; Iwasaki, M.; Tada, H.; Akita, T.; Tanaka, K.; Ito, S. Low-temperature synthesis of anatase–brookite composite nanocrystals: The junction effect on photocatalytic activity. *J. Colloid Interface Sci.* **2005**, *281*, 510–513. [CrossRef] [PubMed]
21. Cao, Y.; Li, X.; Bian, Z.; Fuhr, A.; Zhang, D.; Zhu, J. Highly photocatalytic activity of brookite/rutile TiO_2 nanocrystals with semi-embedded structure. *Appl. Catal. B Environ.* **2016**, *180*, 551–558. [CrossRef]
22. Liu, C.; Yu, T.; Tan, X. Characterization and photocatalytic activity of mixed nanocrystalline TiO_2 powders prepared by xerogel-hydrothermal method in different acid solutions. *Trans. Tianjin Univ.* **2016**, *22*, 473–479. [CrossRef]
23. Rahimpour, A.; Madaeni, S.S.; Taheri, A.H.; Mansourpanah, Y. Coupling TiO_2 nanoparticles with UV irradiation for modification of polyethersulfone ultrafiltration membranes. *J. Membr. Sci.* **2008**, *313*, 158–169. [CrossRef]
24. Miranda-García, N.; Suárez, S.; Sánchez, B.; Coronado, J.M.; Malato, S.; Maldonado, M.I. Photocatalytic degradation of emerging contaminants in municipal wastewater treatment plant effluents using immobilized TiO_2 in a solar pilot plant. *Appl. Catal. B Environ.* **2011**, *103*, 294–301. [CrossRef]
25. Razmjou, A.; Mansouri, J.; Chen, V.; Lim, M.; Amal, R. Titania nanocomposite polyethersulfone ultrafiltration membranes fabricated using a low temperature hydrothermal coating process. *J. Membr. Sci.* **2011**, *380*, 98–113. [CrossRef]
26. Zhang, R.-X.; Braeken, L.; Luis, P.; Wang, X.-L.; Van der Bruggen, B. Novel binding procedure of TiO_2 nanoparticles to thin film composite membranes via self-polymerized polydopamine. *J. Membr. Sci.* **2013**, *437*, 179–188. [CrossRef]
27. Petrochenko, P.; Scarel, G.; Hyde, G.K.; Parsons, G.; Skoog, S.; Zhang, Q.; Goering, P.; Narayan, R. Prevention of ultraviolet (UV)-induced surface damage and cytotoxicity of polyethersulfone using atomic layer deposition (ALD) titanium dioxide. *JOM* **2013**, *65*, 550–556. [CrossRef]
28. Geng, Z.; Yang, X.; Boo, C.; Zhu, S.; Lu, Y.; Fan, W.; Huo, M.; Elimelech, M.; Yang, X. Self-cleaning anti-fouling hybrid ultrafiltration membranes via side chain grafting of poly(aryl ether sulfone) and titanium dioxide. *J. Membr. Sci.* **2017**, *529*, 1–10. [CrossRef]
29. Cruz, N.K.O.; Semblante, G.U.; Senoro, D.B.; You, S.-J.; Lu, S.-C. Dye degradation and antifouling properties of polyvinylidene fluoride/titanium oxide membrane prepared by sol–gel method. *J. Taiwan Inst. Chem. Eng.* **2014**, *45*, 192–201. [CrossRef]
30. Zhao, C.; Xue, J.; Ran, F.; Sun, S. Modification of polyethersulfone membranes—A review of methods. *Prog. Mater. Sci.* **2013**, *58*, 76–150. [CrossRef]
31. Vatanpour, V.; Madaeni, S.S.; Khataee, A.R.; Salehi, E.; Zinadini, S.; Monfared, H.A. TiO_2 embedded mixed matrix PES nanocomposite membranes: Influence of different sizes and types of nanoparticles on antifouling and performance. *Desalination* **2012**, *292*, 19–29. [CrossRef]
32. Teli, S.B.; Molina, S.; Sotto, A.; Calvo, E.G.; Abajob, J.D. Fouling resistant polysulfone–PANI/TiO_2 ultrafiltration nanocomposite membranes. *Ind. Eng. Chem. Res.* **2013**, *52*, 9470–9479. [CrossRef]
33. Zhang, G.; Lu, S.; Zhang, L.; Meng, Q.; Shen, C.; Zhang, J. Novel polysulfone hybrid ultrafiltration membrane prepared with TiO_2-g-HEMA and its antifouling characteristics. *J. Membr. Sci.* **2013**, *436*, 163–173. [CrossRef]
34. Wang, P.; Ma, J.; Shi, F.; Ma, Y.; Wang, Z.; Zhao, X. Behaviors and effects of differing dimensional nanomaterials in water filtration membranes through the classical phase inversion process: A review. *Ind. Eng. Chem. Res.* **2013**, *52*, 10355–10363. [CrossRef]
35. Shi, F.; Ma, Y.; Ma, J.; Wang, P.; Sun, W. Preparation and characterization of PVDF/TiO_2 hybrid membranes with ionic liquid modified nano-TiO_2 particles. *J. Membr. Sci.* **2013**, *427*, 259–269. [CrossRef]
36. Wu, H.; Liu, Y.; Mao, L.; Jiang, C.; Ang, J.; Lu, X. Doping polysulfone ultrafiltration membrane with TiO_2-PDA nanohybrid for simultaneous self-cleaning and self-protection. *J. Membr. Sci.* **2017**, *532*, 20–29. [CrossRef]

37. Zhang, Q.; Fan, L.; Yang, Z.; Zhang, R.; Liu, Y.-N.; He, M.; Su, Y.; Jiang, Z. Loose nanofiltration membrane for dye/salt separation through interfacial polymerization with in-situ generated TiO_2 nanoparticles. *Appl. Surf. Sci.* **2017**, *410*, 494–504. [CrossRef]
38. Yu, J.; Dai, G.; Cheng, B. Effect of crystallization methods on morphology and photocatalytic activity of anodized TiO_2 nanotube array films. *J. Phys. Chem. C* **2010**, *114*, 19378–19385. [CrossRef]
39. Krengvirat, W.; Sreekantan, S.; Mohd Noor, A.-F.; Negishi, N.; Kawamura, G.; Muto, H.; Matsuda, A. Low-temperature crystallization of TiO_2 nanotube arrays via hot water treatment and their photocatalytic properties under visible-light irradiation. *Mater. Chem. Phys.* **2013**, *137*, 991–998. [CrossRef]
40. Wang, D.; Liu, L.; Zhang, F.; Tao, K.; Pippel, E.; Domen, K. Spontaneous phase and morphology transformations of anodized titania nanotubes induced by water at room temperature. *Nano Lett.* **2011**, *11*, 3649–3655. [CrossRef] [PubMed]
41. Liao, Y.; Que, W.; Zhong, P.; Zhang, J.; He, Y. A facile method to crystallize amorphous anodized TiO_2 nanotubes at low temperature. *ACS Appl. Mater. Interfaces* **2011**, *3*, 2800–2804. [CrossRef] [PubMed]
42. Yin, S.; Hasegawa, H.; Maeda, D.; Ishitsuka, M.; Sato, T. Synthesis of visible-light-active nanosize rutile titania photocatalyst by low temperature dissolution–reprecipitation process. *J. Photochem. Photobiol. A Chem.* **2004**, *163*, 1–8. [CrossRef]
43. Yin, S.; Li, R.; He, Q.; Sato, T. Low temperature synthesis of nanosize rutile titania crystal in liquid media. *Mater. Chem. Phys.* **2002**, *75*, 76–80. [CrossRef]
44. Wang, W.; Gu, B.; Liang, L.; Hamilton, W.A.; Wesolowski, D.J. Synthesis of rutile (α-TiO_2) nanocrystals with controlled size and shape by low-temperature hydrolysis: Effects of solvent composition. *J. Phys. Chem. B* **2004**, *108*, 14789–14792. [CrossRef]
45. Karim, M.R.; Bhuiyan, M.T.I.; Dar, M.A.; Seikh, A.H.; Ali Shar, M.; Zaman, M.B.; Lee, C.J.; Kim, H.J.; Lee, M.S. Synthesis and characterization of highly organized crystalline rutile nanoparticles by low-temperature dissolution-reprecipitation process. *J. Mater. Res.* **2015**, *30*, 1887–1893. [CrossRef]
46. Cheng, H.; Ma, J.; Zhao, Z.; Qi, L. Hydrothermal preparation of uniform nanosize rutile and anatase particles. *Chem. Mater.* **1995**, *7*, 663–671. [CrossRef]
47. Wu, M.; Lin, G.; Chen, D.; Wang, G.; He, D.; Feng, S.; Xu, R. Sol-hydrothermal synthesis and hydrothermally structural evolution of nanocrystal titanium dioxide. *Chem. Mater.* **2002**, *14*, 1974–1980. [CrossRef]
48. Yin, H.; Wada, Y.; Kitamura, T.; Kambe, S.; Murasawa, S.; Mori, H.; Sakata, T.; Yanagida, S. Hydrothermal synthesis of nanosized anatase and rutile TiO_2 using amorphous phase TiO_2. *J. Mater. Chem.* **2001**, *11*, 1694–1703. [CrossRef]
49. Yanagisawa, K.; Ovenstone, J. Crystallization of anatase from amorphous titania using the hydrothermal technique: Effects of starting material and temperature. *J. Phys. Chem. B* **1999**, *103*, 7781–7787. [CrossRef]
50. Li, Y.; Fan, Y.; Chen, Y. A novel method for preparation of nanocrystalline rutile TiO_2 powders by liquid hydrolysis of $TiCl_4$. *J. Mater. Chem.* **2002**, *12*, 1387–1390. [CrossRef]
51. Bignold, G.J.; Brewer, A.D.; Hearn, B. Specific conductivity and ionic product of water between 50 and 271 °C. *Trans. Faraday Soc.* **1971**, *67*, 2419–2430. [CrossRef]
52. Yanqing, Z.; Erwei, S.; Zhizhan, C.; Wenjun, L.; Xingfang, H. Influence of solution concentration on the hydrothermal preparation of titania crystallites. *J. Mater. Chem.* **2001**, *11*, 1547–1551. [CrossRef]
53. Jiang, X.; Wang, F.; Li, G.; Qi, L.; Liu, P.; Ding, Y.; Zhang, S.; Yang, M. Low temperature synthesis and mechanism of finely dispersed nanorod rutile titanium dioxide. *RSC Adv.* **2015**, *5*, 62160–62166. [CrossRef]
54. Bharti, B.; Kumar, S.; Kumar, R. Superhydrophilic TiO_2 thin film by nanometer scale surface roughness and dangling bonds. *Appl. Surf. Sci.* **2016**, *364*, 51–60. [CrossRef]
55. Bormashenko, E.Y. *Wetting of Real Surfaces*; De Gruyter: Berlin, Germany, 2013.
56. Wenzel, R.N. Resistance of solid surfaces to wetting by water. *Ind. Eng. Chem.* **1936**, *28*, 988–994. [CrossRef]
57. Cassie, A.B.D.; Baxter, S. Wettability of porous surfaces. *Trans. Faraday Soc.* **1944**, *40*, 546–551. [CrossRef]
58. Li, Y.; Qin, Z.; Guo, H.; Yang, H.; Zhang, G.; Ji, S.; Zeng, T. Low-temperature synthesis of anatase TiO_2 nanoparticles with tunable surface charges for enhancing photocatalytic activity. *PLoS ONE* **2014**, *9*, e114638. [CrossRef] [PubMed]
59. Suttiponparnit, K.; Jiang, J.; Sahu, M.; Suvachittanont, S.; Charinpanitkul, T.; Biswas, P. Role of surface area, primary particle size, and crystal phase on titanium dioxide nanoparticle dispersion properties. *Nanoscale Res. Lett.* **2010**, *6*, 27. [CrossRef] [PubMed]

60. Tian, G.; Fu, H.; Jing, L.; Tian, C. Synthesis and photocatalytic activity of stable nanocrystalline TiO_2 with high crystallinity and large surface area. *J. Hazard. Mater.* **2009**, *161*, 1122–1130. [CrossRef] [PubMed]
61. Akhavan, O. Graphene nanomesh by zno nanorod photocatalysts. *ACS Nano* **2010**, *4*, 4174–4180. [CrossRef] [PubMed]
62. Akhavan, O.; Abdolahad, M.; Esfandiar, A.; Mohatashamifar, M. Photodegradation of graphene oxide sheets by TiO_2 nanoparticles after a photocatalytic reduction. *J. Phys. Chem. C* **2010**, *114*, 12955–12959. [CrossRef]
63. Yuwono, A.H.; Sofyan, N.; Kartini, I.; Ferdiansyah, A.; Pujianto, T.H. Nanocrystallinity enhancement of TiO_2 nanotubes by post-hydrothermal treatment. *Adv. Mater. Res.* **2011**, *277*, 90–99. [CrossRef]
64. Fischer, K.; Gläser, R.; Schulze, A. Nanoneedle and nanotubular titanium dioxide–PES mixed matrix membrane for photocatalysis. *Appl. Catal. B Environ.* **2014**, *160–161*, 456–464. [CrossRef]